PERGAMON

International Journal of Heat and Mass Transfer 45 (2002) 2329–2341

International Journal of HEAT and MASS TRANSFER

www.elsevier.com/locate/ijhmt

Coalescence of bubbles in nucleate boiling on microheaters

Tailian Chen, J.N. Chung *

Department of Mechanical Engineering, University of Florida, P.O. Box 116300, Gainesville, FL 32611-6300, USA

Received 23 May 2001; received in revised form 3 October 2001

Abstract

In this paper, an experiment was performed which is based on a heating surface consisting of microheaters where the temperature of each heater can be individually controlled by an electronic feedback loop. The power consumed by the heaters throughout the cycle of individual bubble growth, coalescence, detachment and departure was measured at high frequencies, thus the heat flux and its variation were obtained. By a careful timing and control of two individual microheaters, we were able to produce two individual bubbles side-by-side. The coalescence would takes place when they grow to a certain size that allows them to touch each other. We have recorded two major heat flux spikes for a typical cycle of boiling with coalescence. The first one corresponds to the nucleation of bubbles; the second one is for the coalescence of the two bubbles. We found that the heat flux variation is closely related to the bubble dynamics and bubble–bubble interaction. By comparing with the single bubble results without coalescence, we also found that the heat transfer is highly enhanced due to the coalescence. © 2002 Published by Elsevier Science Ltd.

1. Introduction

The boiling curve first introduced by Nukiyama [1] has been used to describe the different regimes of saturated pool boiling. In the high-flux nucleate boiling regime, the heat transfer is much higher than other regimes, which explains why the nucleate boiling process is a highly effective heat transfer mode. But until now, there are no theories or literature that exactly explains the underlying heat transfer mechanisms. The suggested theory is that as temperature of the heater surface increases from the onset of nucleate boiling, more bubbles are nucleated and coalesced simultaneously on the heater surface, which further increases the heat flux until the critical heat flux point (CHF) is reached. It has been long thought that bubble–bubble coalescence plays an important, if not dominant, role in the high heat flux nucleate boiling regime and during the CHF condition as well. Because of the microscopic nature and complicated flow and heat transfer mechanisms, the research on coalescence has not progressed very fast in both experimental and theoretical fronts. Coalescence of droplets and bubbles on a surface is a highly complicated process that involves a balance among surface tension, viscous and inertia forces. This phenomenon is intrinsically a fast transient event. Due to the above reasons, the research of coalescence between bubbles has been rather limited. Much of the experimental and numerical work on coalescence in viscous systems is motivated by the sintering process.

Recently, Haddad and Cheung [2] found that the coalescence of bubbles is one of the phases in a cyclic process during nucleate boiling on a downward-facing hemispherical surface. Bubble coalescence follows the phase of bubble nucleation and growth but precedes the large vapor mass ejection phase. A mechanistic model based on the bubble coalescence in the wall bubble layer was proposed by Kwon and Chang [3] to predict the critical heat flux over a wide range of operating conditions for the subcooled and low quality flow boiling. Comparison between the predictions from their model and the experimental CHF data shows good agreement over a wide range of parameters. The model correctly accounts for the effects of flow variables such as pressure, mass flux and inlet subcooling in addition to

* Corresponding author. Tel.: +1-352-392-9607; fax: +1-352-392-1071.

E-mail address: jnchung@ufl.edu (J.N. Chung).

0017-9310/02/$ - see front matter © 2002 Published by Elsevier Science Ltd.
PII: S0017-9310(01)00334-9

Nomenclature

q''	Heat flux (w/cm^2)
$q''_{\text{total (w/o)}}$	Total heat transfer rate per unit area supplied to a heater without boiling (w/cm^2)
$q''_{\text{total (w)}}$	Total heat transfer rate per unit area supplied to a heater with boiling (w/cm^2)
q''_{na}	Heat transfer rate per unit area from a heater due to natural convection (w/cm^2)
q''_{sub}	Heat transfer rate per unit area from a heater due to conduction to substrate (w/cm^2)
q''_{cross}	Heat transfer rate per unit area from a heater due to conduction to the surrounding heaters (w/cm^2)
q''_{rad}	Heat transfer rate per unit area from a heater due to radiation to the ambient (w/cm^2)
q''_{boil}	Heat transfer rate per unit area from a heater due to boiling (w/cm^2)
R	Electrical resistance at temperature T
V	Voltage across the heater
R_0	Resistance at ambient temperature T_0
A	Heater surface area (cm^2)
C	Platinum constant coefficient (Ω/Ω °C)
T	Heaters temperature (°C)
T_0	Ambient temperature (°C)

geometry parameters. Ohnishi et al. [4] investigated the mechanism of secondary bubble creation induced by bubble coalescence in a drop tower experiment. They also performed a two-dimensional numerical simulation study. They reported that the simulation results agree well with the experimental data and indicate that the size ratio and the non-dimensional surface tension play the most important role in the phenomena. Bonjour et al. [5] reported a study of the coalescence phenomenon (merging of two or more bubbles into a single larger one) during pool boiling on a duraluminium (AU4G) vertical heated wall. They investigated various boiling curves characterizing boiling (with or without coalescence) for three artificial nucleation sites which are spaced at variable distances apart. In their experiment, the heat flux ranges from 100 to 900 w/cm^2 and the wall superheat from 5 to 35 K. They pointed out that the coalescence of bubbles results in higher heat transfer coefficients than single-site boiling. They also showed that coalescence results in a decrease in the bubble frequency. In a numerical study, Yang et al. [6] performed a numerical study to investigate the characteristics of bubble growth, detachment and coalescence on vertical, horizontal, and inclined downward-facing surfaces. The FlowLab code, which is based on a lattice-Boltzmann model of two-phase flows, was employed. Macroscopic properties, such as surface tension and contact angle, were implemented through the fluid–fluid and fluid–solid interaction potentials. The model predicted a linear relationship between the macroscopic properties of surface tension and contact angle, and microscopic parameters. Hydrodynamic aspects of bubble coalescence are investigated by simulating the growth and detachment behavior of multiple bubbles generated on horizontal, vertical, and inclined downward-facing surfaces. For the case of horizontal surface, three distinctive regimes of bubble coalescence were represented in the lattice-Boltzmann simulation: lateral coalescence of bubbles situated on the surface, vertical coalescence of bubbles detached in a sequence from a site, and lateral coalescence of bubbles, detached from the surface. Multiple coalescence was predicted on the vertical surface as the bubble detached from a lower elevation merges with the bubble forming on a higher site. The bubble behavior on the inclined downward-facing surface was represented quite similar to that in the nucleate boiling regime on a downward-facing surface. Frenkel [7] posed the problem of the merging of two spheres with a slow fluid motion as the first step towards understanding the viscous coalescence mechanisms. For the coalescence of liquid drops, viscosity plays a dominant role. The experimental work of Bradley and Stow [8] on the coalescence of water drops shows that the low viscosity of water makes the motion very rapid and difficult to observe. On the other hand, by using a very high-viscosity fluid, the motion can be slowed for better visualization in the experiment of Brinker and Scherer [9] and their experimental results agree very well with numerical simulations of the Stokes equations [10]. Eggers et al. [11] found that when two drops of radius R touch each other, surface tension drives an initially singular motion which joins them into a bigger drop with smaller surface area. This motion is always viscously dominated at early times. They focus on the early-time behavior of the radius r_m of the small bridge between the two drops. The flow is driven by a highly curved meniscus of length $2\pi r_m$ and width $\Delta \ll r_m$ around the bridge, from which they conclude that the leading-order problem is asymptotically equivalent to its two-dimensional counterpart. Sakashita and Kumada [12] proposed that the CHF be caused by the dryout of a liquid layer formed on a heating surface. They also suggested that a liquid

macrolayer is formed due to the coalescence of bubbles for most boiling systems, and that the dryout of the macrolayer is controlled by the hydrodynamic behavior of coalesced bubbles on the macrolayer. Based on these considerations, a new CHF model is proposed for saturated pool boiling at higher pressures. In the model, they suggest that a liquid macrolayer be formed due to coalescence of the secondary bubbles formed from the primary bubbles. The detachment of the tertiary bubbles formed from the secondary bubbles determines the frequency of the liquid macrolayer formation. The CHF occurs when the macrolayer dries out before the departure of the tertiary bubbles from the heating surface. One of the formulations of the model gives the well-known Kutateladze or Zuber correlation for CHF in saturated pool boiling. The vast majority of experimental work performed to date utilized the heat flux-controlled heater surface to generate bubbles. Rule and Kim [13] were the first to utilize microheaters to obtain a constant temperature surface and produced spatially and temporally resolved boiling heat transfer results. Bae et al. [14] used identical microheaters as those by Rule and Kim [13] to study single bubbles during nucleate boiling. They performed heat transfer measurement and visualization of bubble dynamics. In particular, it was found that a large amount of heat transfer was associated with bubble nucleation, shrinking of dry spot before departure, and merging of bubbles. In the current work, identical microheaters as those developed by Rule and Kim [13] were used to study the coalescence of two individual bubbles. For each experiment, the temperature of the heaters was kept constant while the time-dependent heat flux and bubble images were recorded. The objective of this study is to establish a correlation between the bubble–bubble interaction and the local heat flux responses at given heater temperatures. To accomplish this experimentally, the heat flux from the heater surface and the bubble–bubble coalescence interaction are obtained simultaneously. This leads to the following advantages:

1. The time-dependent heat flux variation during the bubble's life cycle can be obtained.
2. It is possible to produce bubble–bubble coalescence in a controlled and repeatable manner and observe heat flux variation during bubble coalescence.

2. Experimental system

2.1. Heaters array

Shown in Fig. 1 is the heater array used in this experiment (see [13] for details). There are 96 heaters in the array, each of which is individually controlled by a feedback electronic circuit shown in Fig. 2. The size of each individual heater is 270 μm × 270 μm.

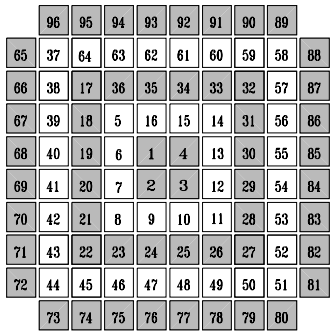

Fig. 1. Heaters array.

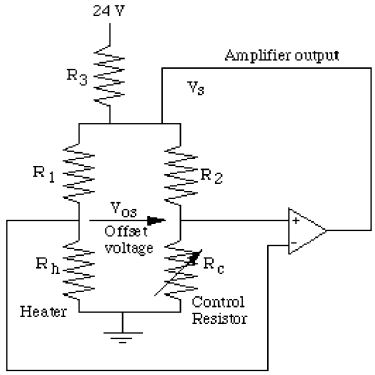

Fig. 2. Wheatstone bridge control circuit diagram.

2.2. Heater temperature control

This experiment makes use of the relationship between platinum's electrical resistance and temperature. We know that the resistance of the platinum varies almost linearly with its temperature by the following relationship:

$$(R - R_0)/R = C(T - T_0), \tag{1}$$

where R is the electrical resistance at temperature T, R_0 is the resistance at a reference temperature T_0. C is the constant coefficient. For platinum, the value of C is 0.002 Ω/Ω °C.

In this experiment, each heater's nominal resistance is 750 Ω. For a temperature change of 1 °C, the heater's resistance would change by 1.5 Ω. Each heater has an electronic loop to regulate and control the voltage across it. The Wheatstone bridge shown in Fig. 2 is used to carry out the constant temperature control. R_h is the platinum heater resistance while R_1, R_2, R_3 are normal metal film resistors whose values are not sensitive to temperature. R_c is the control heater resistance which is set by the computer. The bridge is said to be balanced when $V_{os} = 0$. This occurs when the ratio between R_1 and

R_h is the same as that between R_2 and R_c. The feedback loop maintains the heater at a constant temperature by detecting imbalance and regulating the current through the bridge in order to bring it back into balance. The amplifier will increase or decrease the electrical current to the circuit until the heater reaches the resistance necessary for the bridge to maintain the balance. Therefore, the exact value of R_c corresponds to the temperature of the heater R_h. Thus, in our experiment, we need to find a control resistance value R_c which corresponds to the temperature of the heater R_h. This is accomplished by calibration.

2.3. Heater calibration

To set the heaters at a certain temperature, a relationship between the control resistance R_c and heater temperature is needed. One method is to calculate the heater temperature based on the relationship of Eq. (1). But a more reliable method was to calibrate the control resistance of R_c directly with the heater temperature. This was performed according to the following procedure. An insulated, circulating constant temperature oil bath was heated to the desired calibration temperature within 0.2 °C, and the heater array was sprayed with the oil onto its surface. The control resistance R_c was initially set at a low value, so the voltage across the heater was at its minimum value. The control resistance R_c was incremented until the voltage across the bridge approached zero and the amplifier began to regulate the heater resistance by applying power to the top of the bridge circuit (Fig. 2). The other heaters were calibrated by the same procedure. It is worth mentioning that different heaters in the heater array may have different control resistance values R_c for a certain temperature, due to various factors affecting the system, mainly different electrical resistances for different heaters, though they have their own nominal values. But in calibration, the control resistance values will incorporate all those factors.

2.4. Boiling condition

In this experiment, we chose FC-72 to be the boiling fluid. The reason is that it is dielectric, which makes it possible for each heater to be individually controlled. The bulk fluid is at the room condition (1 atm, 25 °C), where its saturation temperature is 56 °C [15], thus it is subcooled pool boiling.

2.5. Data acquisition

To investigate the bubbles' coalescence, we need to generate single bubbles on different heaters. Since each of the 96 heaters on the heater array is individually controlled by the electronic feedback control system, we can set active one or more of the heaters by powering them individually so that they reach a certain temperature while leaving all other heaters unheated. In some experiments, in reference to Fig. 1, if only two adjacent heaters are powered, such as #1 and #3, or #1 and #2, the coalescence of bubbles is not distinguishable. On the other hand, powering two heaters which are further apart, such as #1 and #25, two single bubbles will be generated, but the bubbles' departure sizes are not large enough for them to touch and merge before they depart. Therefore, for coalescence to take place, the active heaters have to be far enough to allow both bubbles to be distinguished while close enough for coalescence to occur. By trial and error, heater pair #1 and #11, and pair #1 with #12 were found to provide satisfactory results. First each heater was allowed to remain at a set temperature for about 15 min to reach steady state. Then the voltage across each heater during experiments was acquired at a sampling rate of 40,000 Hz into computer through data acquisition system, which is shown in Fig. 3. The data was found to be repeatable under these conditions. The acquired voltages were converted to heat flux from the heaters according to the following basic relationship:

$$q'' = (V^2/R)/A. \tag{2}$$

To investigate the effect of bubble–bubble coalescence on boiling heat transfer, we first performed single bubble boiling. That is, we powered heaters #1, #11 and #12, respectively, so that the single bubbles nucleate, grow and depart without coalescence. After the single bubble boiling, for two heater pairs #1 with #11, and #11 with #12, we generated individual bubbles on the two heaters simultaneously and allowed them to coalesce. In each of the coalescence experiments, both heaters are always set at the same temperature, and their temperature were set from 100 to 140 °C with an increment of 5 °C. The bubbles were nucleated on each heater at approximately the same time. They grew to a certain size and coalesced. For both single-bubble and coalescence cases, we obtained the voltages across the

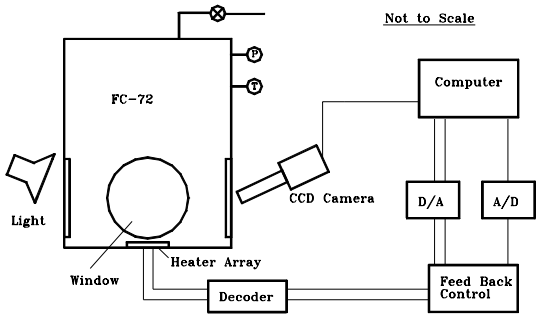

Fig. 3. Experiment Apparatus.

heaters. In the meantime, the visualization of bubbles' behavior by a fast CCD camera was intended to gather more information.

3. Data reduction

3.1. Qualitative heat transfer analysis

As indicated above, each microheater has a dimension of 270 μm × 270 μm. From an overall point of view, each heater is just a "point" compared with the entire heater array. By powering a point heater and setting it at a temperature sufficient to generate single bubbles on its surface, the heat transfer is quite different from that on a large surface due to the edge effect. Therefore, its boiling behavior is different from that on a large heater surface.

Referring to Fig. 4, heat transfer from the point heater is composed of the following:

1. Conduction to the substrate on which the heater is mounted. This is due to the temperature gradient between the heater and the ambient through the substrate.

2. Boiling heat transfer on top of the submerged horizontal heater surface during the boiling experiment when the boiling chamber is positioned as shown in Fig. 3 and the heaters array is mounted at the bottom of the chamber. This boiling heat transfer is replaced by the natural convection between the heater and the air and FC-72 vapor mixture when the chamber is tilted 90° so that the heater is oriented vertically and separated from the liquid for data reduction experiment.

3. Heat conduction to the surrounding heaters. When all heaters in the heater array are set at a certain constant temperature, the heater array is a constant temperature surface. In this case, there is little heat conduction to the surrounding heaters. But in the case of a single heater, since all other heaters are unheated, there is significant heat conduction between the point heater and the surrounding heaters.

4. Radiation from the heater surface. Since the temperature range of interest in this experiment is not very high, this part of the heat transfer is very small compared with others. As discussed next, its effect on boiling heat transfer is completely eliminated.

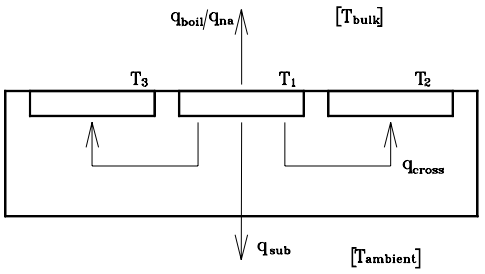

Fig. 4. Single heater schematic.

3.2. Data reduction procedure

To obtain the heat transfer rates due to boiling only, we conduct the experiments according to the following procedure:

1. Measure the total power supplied to the heater during the boiling process at different heater temperatures.

The total heat flux with boiling present is:

$$q''_{\text{total(w)}} = q''_{\text{sub}} + q''_{\text{cross}} + q''_{\text{rad}} + q''_{\text{boil}}. \tag{3}$$

2. Tilt the boiling chamber 90°, so that the heater array is removed from the liquid and exposed to the air and FC-72 vapor. While separated from the FC-72 liquid, we measure the total heat flux without boiling at corresponding temperatures.

This total heat flux without boiling present is:

$$q''_{\text{total (w/o)}} = q''_{\text{na}} + q''_{\text{sub}} + q''_{\text{cross}} + q''_{\text{rad}}. \tag{4}$$

The conduction to the substrate q''_{sub} in Eqs. (3) and (4) should be identical because the heater is set at the same temperature. Since the conduction to the neighboring heaters q''_{cross} are approximately the same, the boiling heat transfer is obtained by computing the difference between Eqs. (3) and (4) as follows:

$$q''_{\text{boil}} = q''_{\text{total (w)}} - q''_{\text{total (w/o)}} + q''_{\text{na}}. \tag{5}$$

The natural convection component in Eq. (5) was calculated using the correlation of Churchill and Chu [16] for flat, vertical, isothermal heaters.

3.3. Uncertainty analysis

The uncertainties in this experiment include heater temperature and heat flux measurements.

The uncertainties in temperature arise from the following:

1. The circuit that maintains the heater temperature exhibits offset voltage drift due to the inherent nature of operational amplifier (LTC1150) as shown in Fig. 2. It has an offset voltage of 0.5 μV and a drift of 0.01 μV/°C. The slew rate is 3 V/μs. The temperature uncertainty due to this drift was estimated to be 0.4 to 0.6 °C [13].

2. Uncertainty arises in controlling the bulk fluid temperature, which was seen to vary during a 10 h run by about ±0.5 °C.

The uncertainty associated with determination of the total boiling heat flux comes mainly from the data reduction as outlined in Section 3.2, since the heat flux is directly calculated from the voltages across the heaters. Based on the assumptions mentioned in Section 3.2, the

uncertainty estimate for heat flux has been done by using the method of Kline and McClintock [17], with odds (20:1), 90% confidence level, which is about ±30%.

4. Results and analysis

4.1. Single bubble boiling

Fig. 5 shows the heat flux history of heater #1 when single bubbles are nucleated on this heater at different heater surface temperatures. Fig. 6 shows the average heat flux for a single bubble boiling from heaters #1, #11 and #12, respectively. Figs. 7(a)–(c) are the typical bubble ebullition cycle when the bubbles experience nucleation, growth, detachment and departure. From

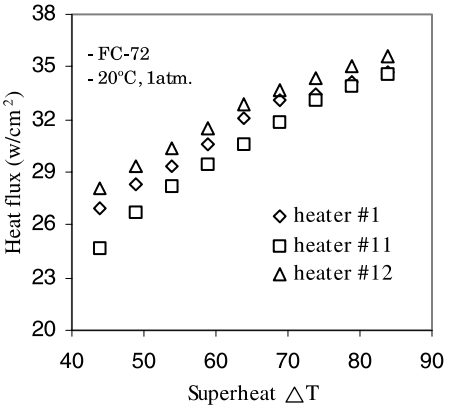

Fig. 6. Single bubble boiling at different superheats.

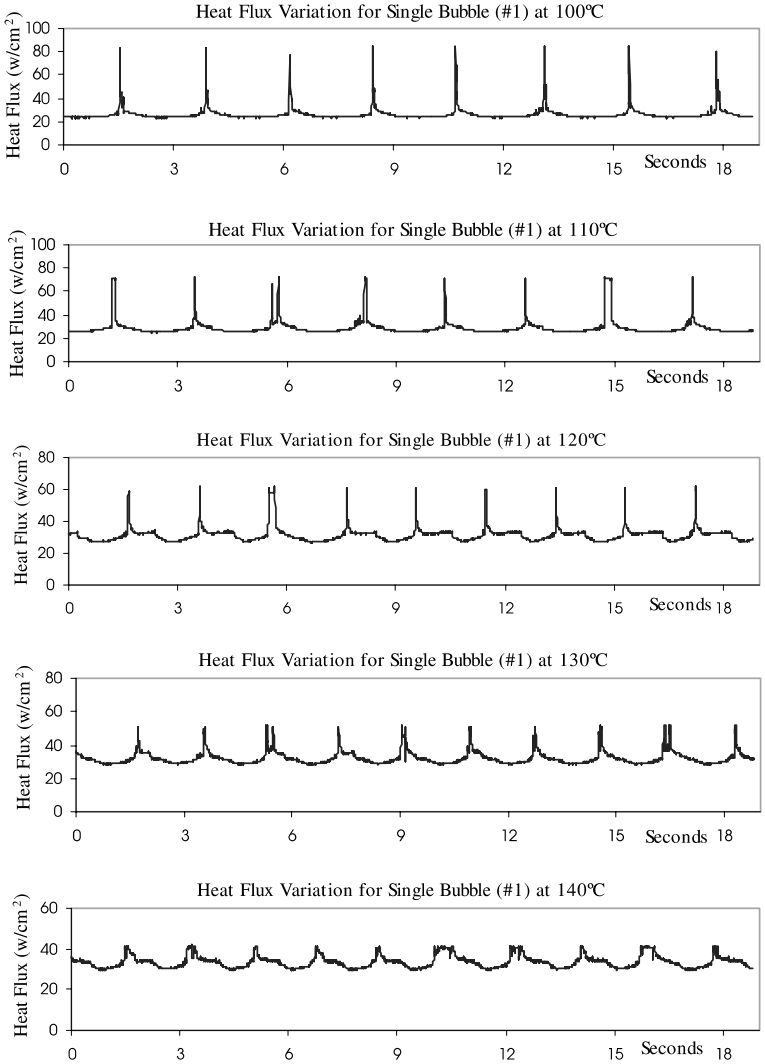

Fig. 5. Heat flux variation at different temperatures.

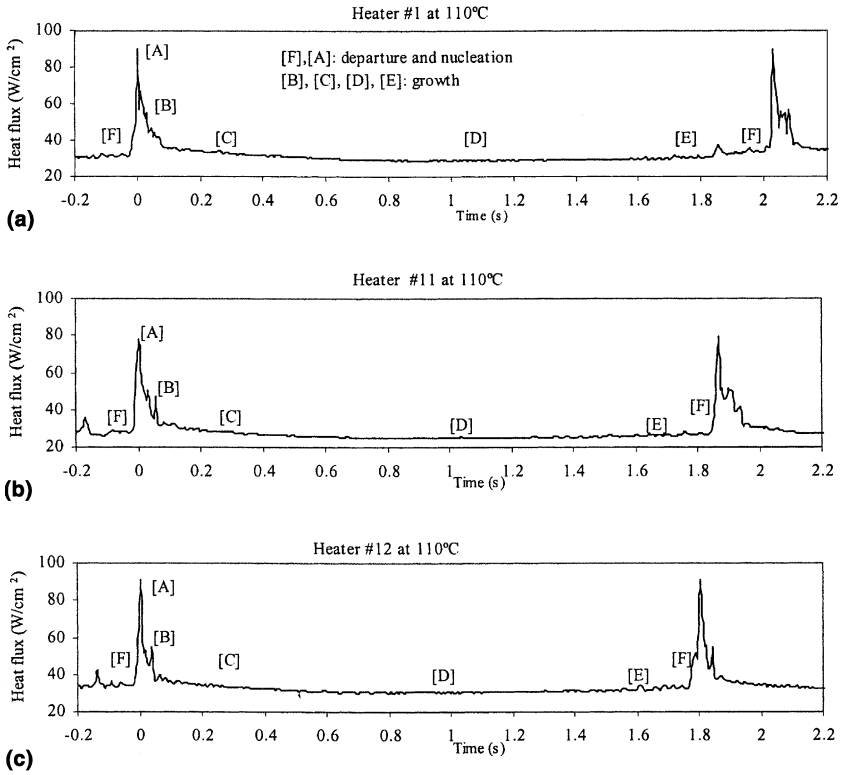

Fig. 7. Heat flux variation during one bubble life cycle (a) heater #1, (b) heater #11, (c) heater #12.

Figs. 5–7, we have the following observations and analysis:

1. From Fig. 5, where each spike represents the departure of a bubble, we can conclude that the bubble departure frequency increases with heater temperature. At a heater temperature of 100 °C, about eight bubbles departed within 18.8 s, while at 140 °C, 10 bubbles departed within the same period of time. As shown in Fig. 6 the heat transfer is higher at a higher heater temperature which produces more bubbles in the same time period. Fig. 5 also demonstrates the repeatability of the experiment.

2. From Fig. 6, we found that the average heat flux increases as the heater temperature is increased. This is consistent with the results obtained by the previous investigators for large heater surfaces. For large heater surfaces, the resulting increase in heat flux with increasing heater temperature has been explained due to the increase of nucleation sites, and coalescence among the more and more bubbles on the heater surfaces. However, in addition to the more microscopic active nucleation sites on one single heater, this heat flux increase for microheater in this experiment can possibly be due to larger conduction to the vapor in the bubble, and the higher evaporation rate in the microlayer.

3. From Fig. 7, we note that the heat flux is closely associated with the bubble life cycle during the ebullition process. [A] corresponds to the largest spike which takes place during the bubble departure. When the preceding bubble departs, the heater is rewetted by the cooler bulk fluid. The establishment of the microlayer for the succeeding new bubble on the heater surface and the turbulent convection induced by this vapor–liquid exchange lead to this large heat flux spike. [B] represents the moment when the succeeding bubble starts to grow after the vapor–liquid exchange. As the new bubble grows, the contact line which is the three-phase division expands outward. The bubble growth results in a larger dry area on the heater surface, thus the heat flux is decreasing. The low heat flux period indicated by [D], [C] and [E] corresponds to the slow growth stage of a bubble. As the size reaches a certain level, the buoyancy force starts to become more important than the forces which hold the bubble to the surface, but it is still not large enough to lift the bubble from the heater surface, causing the bubble to neck. During the necking process, the contact line starts to shrink, then the dryout area is starting to decrease, thus we have observed that the heat flux is starting to increase slightly with some oscillation of a small amplitude. Finally, the buoyancy force is large

enough to detach the bubble from the heater surface, and then another bubble ebullition cycle begins.

4. Based on the heat flux history, the bubble life cycle can be categorized into the following periods: nucleation, growth, detachment, and departure. This detachment force results in a bottle-neck connecting the new bubble embryo with the to-be-departing bubble as Fig. 8 shows. The detachment also leaves room for the new bubble to grow. During the detachment process, the bubble disjoining force with the substrate surface becomes small so that the net force imbalance on the detaching bubble makes it vibrate substantially, thus causing the heat flux to fluctuate.

5. We observed that the bubble departing size increases as the heater temperature increases. The buoyancy force, besides the inertia force of the bubble, is primarily responsible for the bubble departure. The interfacial surface tension along the contact line invariably acts to hold the bubble in place on the heater surface. Since surface tension increases with temperature, for departure to occur at higher heater temperatures, a larger bubble size is required to overcome the adhesive force. Also, at higher temperatures, the thermal boundary layer of the liquid phase next to the heater is thicker, which allows the bubble to grow larger.

6. As the heater temperature increases, the maximum heat flux during bubble departure decreases and the minimum heat flux increases, which occurs in the low-heat flux bubble growth regime. The decrease of the maximum heat flux is thought to be due to the larger bubble departing size, which results in a larger bubble embryo left on the substrate surface creating a larger dry area on the heater surface. Heat transfer is very low on the dry surface. For the low-heat flux growth regime, most of the heater area is covered with vapor, the conduction to the vapor inside the bubble is dominant, which is proportional to the heater surface temperature.

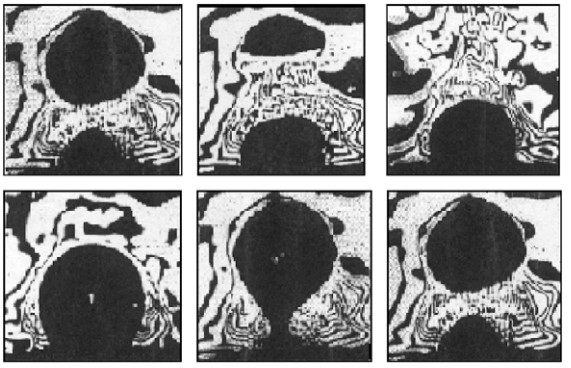

Fig. 8. Bubble ebullition process (from Dieter Nordmann und Franz Mayinger, Temperatur, Druck und Warmetransport in der Umgebung kondensierender Blasen, VDI-Forschungsheft 605, 1981).

In summary, we observed one heat flux spike during a single bubble boiling cycle, the heat flux is closely associated with the dry area on the heater surface. The average and minimum heat fluxes increase as the heater temperature increases, though the maximum heat flux decreases as the temperature increases.

4.2. Dual bubble boiling with coalescence

We used two heater configurations for the coalescence study. Heater #1 was paired with #11 for the first case and it was then paired with #12 for the second. For each pair of heaters, single bubbles were generated on each heater and then synchronized such that coalescence would take place from the two bubbles generated by the heater pair. Fig. 9 shows the heat flux variations with time registered by each heater during the coalescence. Fig. 10 shows one typical ebullition cycles for each heater in the two configurations. Together with visualization results, we observed that one ebullition cycle with coalescence spans from [A] to [F], where [A]–[C] is the single bubble period before coalescence. [D] is associated with the bubbles coalescence moment. After this point, the newly coalesced bubble grows till the departing point [F]. After this, another cycle starts. The details of this process are as follows:

[A]: This point corresponds to the nucleation of the new bubble. Similar to the single bubble boiling presented above, we observed a heat flux spike after the bubble departure.

[B],[C]: This portion corresponds to the low-heat flux growth period. The mechanism is the same as the single bubble boiling at the same stage discussed before.

[D]: This point corresponds to the moment when the two bubbles coalesce. The coalescence also produced a major heat flux spike. When the two bubbles grow to a certain size where their boundaries contact each other, the two bubbles then merge and form a new bubble. It is due to the interfacial surface tension and the Marangoni convection that make the newly coalesced bubble stay on top of the two heaters. Because the power sources are from two single heaters, the new coalesced bubble forms an oval shape with its major axis in the direction of two heaters. The heaters are rewetted with liquid again and part of heaters is in the microlayer region, thus resulting in the heat flux spike. To make clearer the coalescence process, we take a look at the heater arrangement in Fig. 11. Just before the coalescence as shown in Fig. 11(a), the individual bubbles are sitting on their respective heaters. The dry area indicated by the contact line covers most of the heater area. Only a small portion of the heater area is wetted with liquid in the microlayer region. After the coalescence, as Fig. 11(b) shows, a large portion of the heaters is rewetted with liquid again, which results in a high evaporation rate, thus heat flux

maintains at a higher level which is indicated as region [E] in Fig. 10.

[E]: This is the low-heat flux growth period for coalesced bubble. Compared to the heat flux before coalescence for bubble growth, the heat flux is now higher. We also noticed from Fig. 10 that there is substantial heat flux fluctuation after coalescence. The instability of liquid film beneath the coalesced bubble, the formation of microbubbles and the large volume of the merged bubble are all possible causes for the heat flux fluctuation.

[F]: This corresponds to the moment when the coalesced bubble departs from the heater surface and the start of a new cycle.

From the foregoing analysis and a comparison with the case without coalescence, it is clear that during the boiling cycle the bubble departure and new bubble nucleation result in one major heat flux spike, whereas for the case with coalescence, it is obvious that there are two major spikes during an ebullition cycle. The first is due to the bubble departure and the second is due to the coalescence of the bubbles. After the coalescence, the heat flux maintains at a higher level than that before the coalescence.

For each heater pair, the heaters were set at the same temperature during a particular coalescence experiment. For the entire study, the temperatures of the heaters were varied from 100 to 140 °C. Figs. 12 and 13 show the average heat flux for a heater during an ebullition cycle at different heater temperatures. Fig. 12 is for heater pair #1 with #11, and Fig. 13 is for #1 with #12. These results were obtained by dividing the total power dissipation by the two heaters total area. We have the following observations:

1. In general, the average heat flux increases with heater temperature as expected. Also the entire curve resembles the macroscopic pool boiling curve introduced by Nukiyama [1] where the heat flux would decrease after reaching a local maximum (critical heat flux in regular pool boiling). After reaching a local minimum (Leidenfrost point in regular pool boiling), the heat flux would resume a positive slope.

2. It is noted that for heater pair #1 with #12, the region between local maximum and local minimum in heat fluxes is not as distinctive as pair #1 with #11. It also occurs at different temperatures. We speculate that because the separation distance between #1 and #12 is shorter than that between #1 with #11, there is

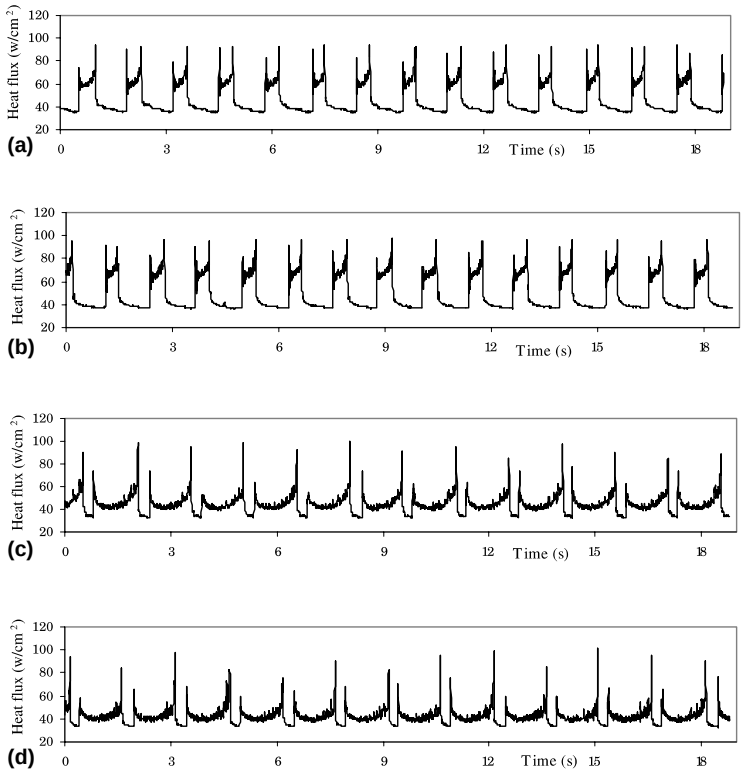

Fig. 9. (a) The heat flux variation for #1, when coalesce with #11 at 110 °C. (b) The heat flux variation for #11, when coalesce with #1 at 110 °C. (c) The heat flux variation for #1, when coalesce with #12 at 100 °C. (d) The heat flux variation for #12, when coalesce with #1 at 100 °C.

more dry area for pair #1 and #12. On the other hand, different heater areas for #1 and #12 might have contributed to the difference. Heater #2 (0.0748 mm^2) has a larger area than # 1 (0.07316 mm^2), while #1 and #11 (0.0732 mm^2) are much closer in surface areas.

4.3. Heat transfer enhancement due to coalescence

The main objective of the current study is to investigate the effect of coalescence on boiling heat transfer. To quantitatively compare the heat transfer between the single bubble case and that with coalescence, we use the same method to obtain the average heat flux for the single bubble boiling at the same boiling conditions. Fig. 14 shows the heat transfer enhancement for heater pair #1 with #11, in which Fig. 14(a) is the absolute heat flux increase and Fig. 14(b) is the percent increase. Fig. 15 is for the heater pair #1 with #12. For pair #1 with #11, the heat transfer enhancement changes substantially with the heater temperature, while for pair #1 with #12, the heat transfer enhancement is relatively insensitive to the heater temperature. Apparently the enhancement curves carry some similarity to those boiling curves with coalescence in Figs. 12 and 13.

4.4. Bubble departure frequency

Fig. 16 is plotted to compare the bubble departure frequencies for the coalescence case with that without coalescence. It illustrates the heat flux variation during a

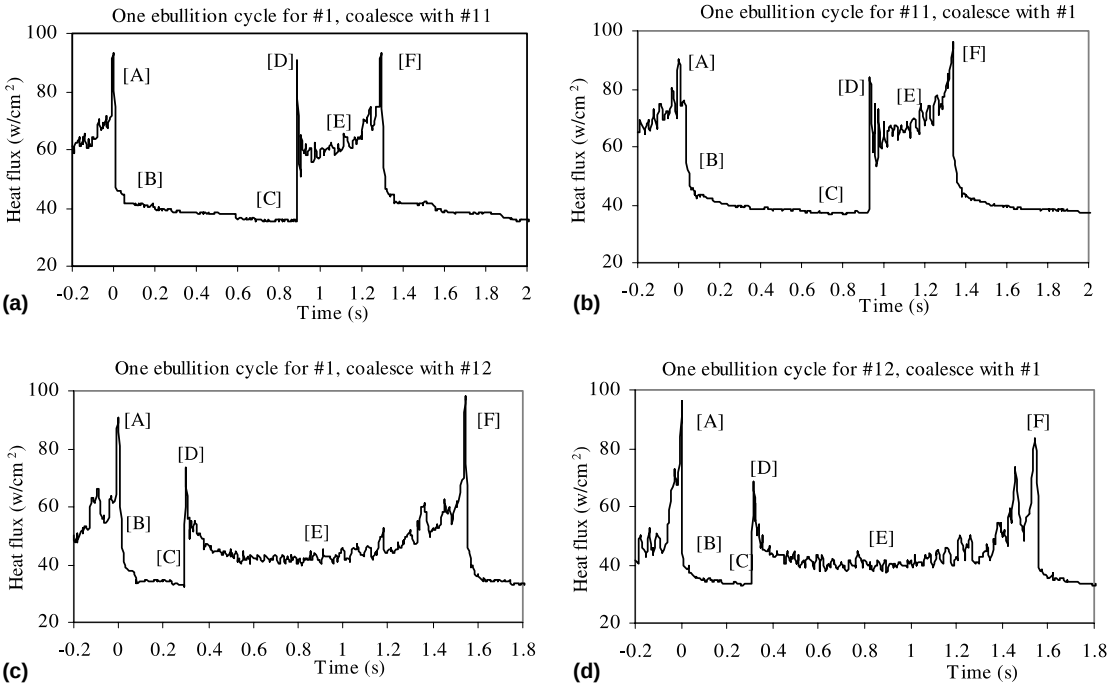

Fig. 10. One typical ebullition bubble cycle for two configurations, (a) and (b) for heater #1 with #11, (c) and (d) for heater #1 with #12.

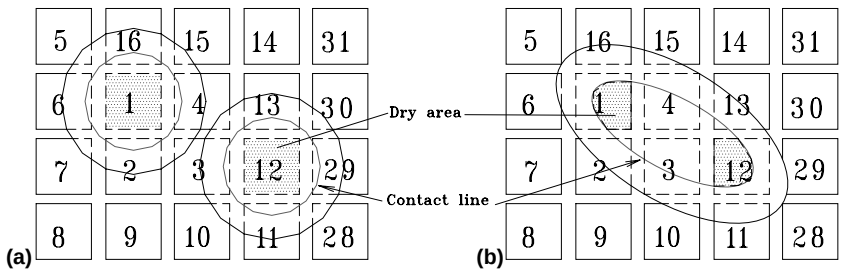

Fig. 11. The heaters dry area before and after coalescence.

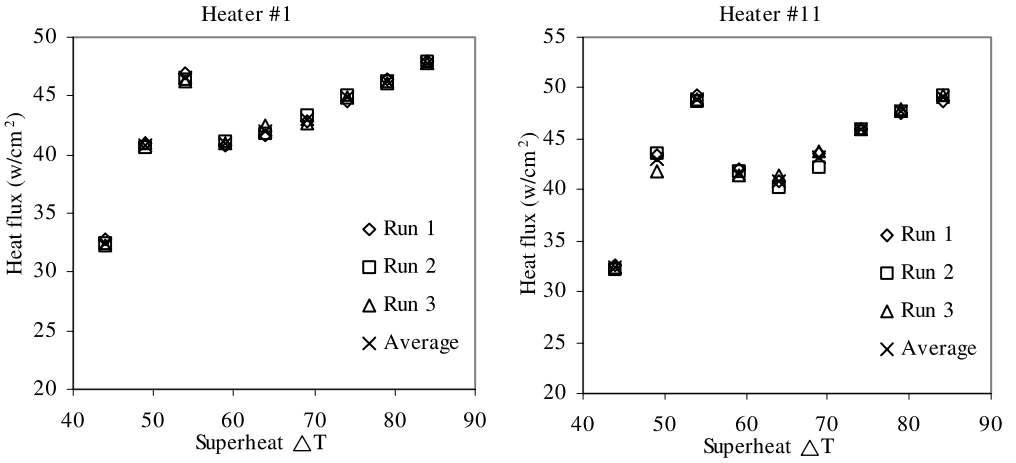

Fig. 12. The boiling heat flux for heater #1 and #11 at different temperatures as they are set different temperatures to generate bubbles and coalesce.

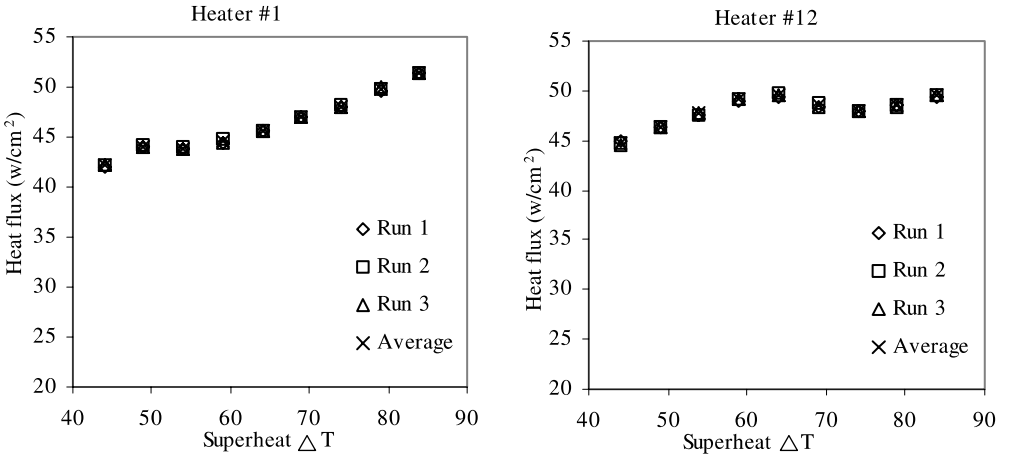

Fig. 13. The boiling heat flux for heater #1 and #12 at different temperatures as they are set different temperatures to generate bubbles and coalesce.

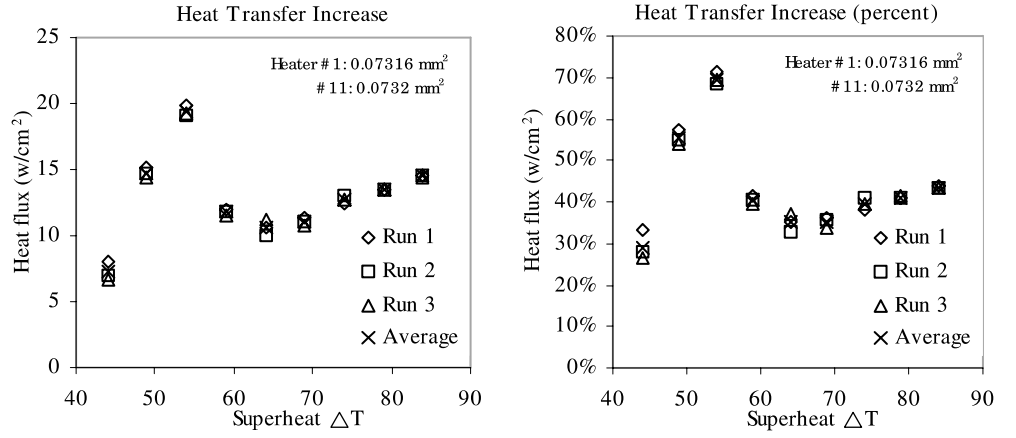

Fig. 14. The heat flux increase due to coalescence (#1 with #11).

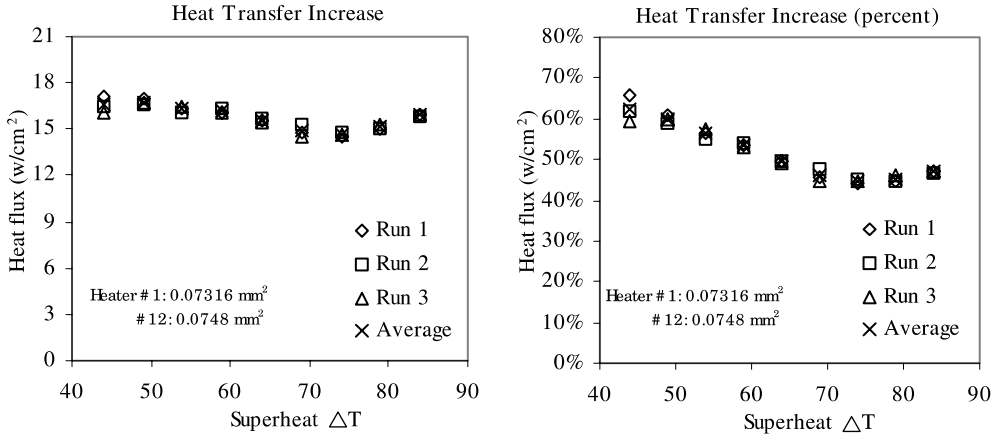

Fig. 15. The heat flux increase due to coalescence (#1 with #12).

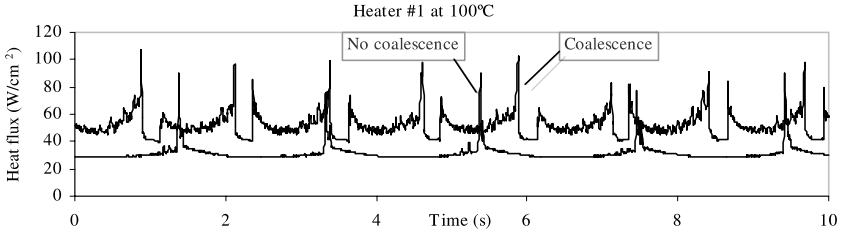

Fig. 16. Heater transfer from heater #1 for coalescence and non-coalescence cases.

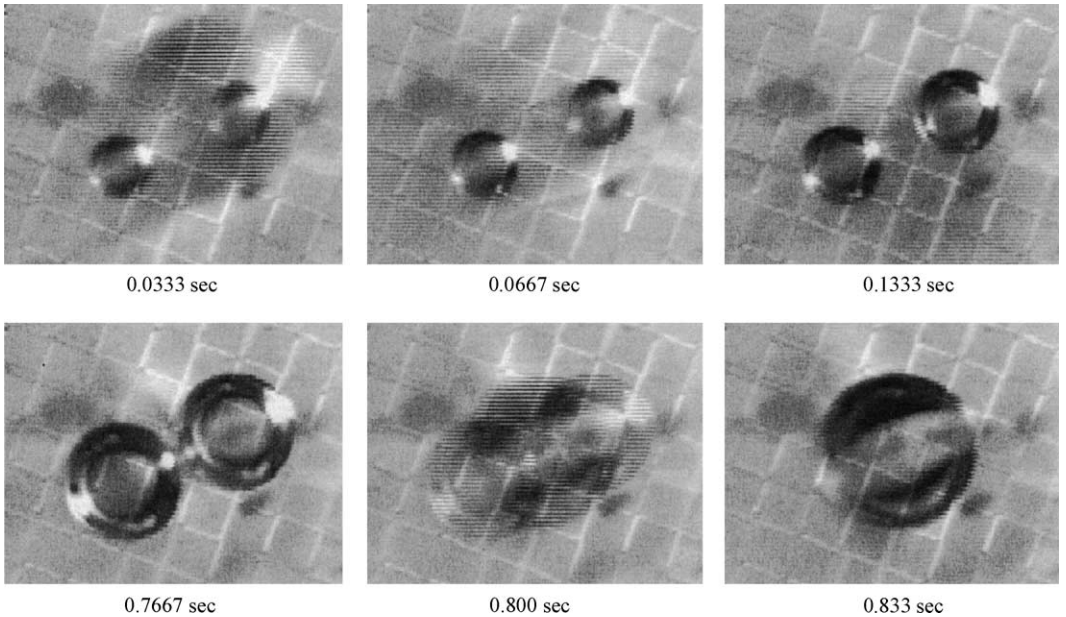

Fig. 17. Visualization of bubble coalescence process (images taken from the bottom of heaters).

10-second period, which also indicates the bubble life cycles for the single bubble case and the bubble–bubble coalescence case. It is clear that when two bubbles coalesce, the departure frequency increases as a result of enhanced heat transfer.

4.5. Visualization of bubble coalescence

Fig. 17 provides a photographic visualization of the coalescence process from beneath the microheaters. The bubble growth process is also shown in the photographs. It is clear that the two bubbles are quite identical which results in a symmetric coalescence process.

5. Summary and conclusions

Comparing the heat transfer characteristics during coalescence with those for the single bubble case, we offer the following summary and conclusions:

1. There are two major heat flux spikes for the case with coalescence as compared to only one single major spike for the non-coalescence case. Through a quantitative analysis, coalescence results in a substantial heat transfer enhancement.
2. The bubble departure frequency increases due to coalescence of bubbles as compared with the single bubble case at the same boiling condition.
3. The boiling heat transfer is closely associated with the bubble's contact line movement and dry area on the heater surface.
4. The heat transfer rate during bubble growth after coalescence is larger than that before coalescence.
5. Degree of heat transfer enhancement depends on the configuration and temperature of the two heaters.

Acknowledgements

The technical assistance and fruitful discussion offered to us by Dr. Jungho Kim of the University of Maryland are greatly acknowledged. This research was made possible by the Andrew H. Hines, Jr./Florida Progress Endowment Fund.

References

[1] S. Nukiyama, The maximum and minimum values of heat transmitted from metal to boiling water under atmospheric pressure, J. Jpn. Soc. Mech. Eng. 37 (1934) 367–374 (Translated in Int. J. Heat Transfer 9 (1966) 1419–1433).
[2] K.H. Haddad, F.B. Cheung, Steady-state subcooled nucleate boiling on a downward-facing hemispherical surface, J. Heat Transfer-Trans. ASME 120 (1998) 365–370.
[3] Y.M. Kwon, S.H. Chang, A mechanistic critical heat flux model for wide range of subcooled and low quality flow boiling, Nucl. Eng. Des. 188 (1999) 27–47.
[4] M. Ohnishi, H. Azuma, J. Straub, Study on secondary bubble creation induced by bubble coalescence, Gravitational Eff. Mater. Fluid Sci. 24 (1999) 1331–1336.
[5] J.M. Bonjour, M. Clausse, M. Lallemand, Experimental study of the coalescence phenomenon during nucleate pool boiling, Exp. Thermal Fluid Sci. 20 (2000) 180–187.
[6] Z.L. Yang, T.N. Dinh, R.R. Nourgaliev, B.R. Sehgal, Numerical investigation of bubble coalescence characteristics under nucleate boiling condition by a lattice-Boltzmann model, Int. J. Thermal Sci. 39 (2000) 1–17.
[7] J. Frenkel, Viscous flow of crystal-line bodies under the action of surface tension, J. Phys. 9 (1945) 385–391.
[8] S.G. Bradley, C.D. Stow, Collision between liquid drops, Phil. Trans. R. Soc. London A 287 (1978) 635–675.
[9] C.J. Brinker, G.W. Scherer, Sol-Gel Science, Academic Press, New York, 1990.
[10] J.I. Martinez-Herrera, J.J. Derby, Viscous sintering of spherical particles via finite element analysis, J. Am. Ceram. Soc. 78 (1995) 645–649.
[11] J. Eggers, J.R. Lister, H.A. Stone, Coalescence of liquid drops, J. Fluid Mech. 401 (1999) 293–310.
[12] H. Sakashita, T. Kumada, A new model for CHF in pool boiling at higher pressure, JSME Int. J. Ser. B-fluids Thermal Eng. 36 (1993) 422–428.
[13] T.D. Rule, J. Kim, Heat transfer behaviour on small horizontal heaters during pool boiling in FC-72, J. Heat Transfer 121 (1999) 386–393.
[14] S.W. Bae, J. Kim, J.D. Mullen, M.H. Kim, Preliminary wall heat transfer measurements and visualization of bubble growth and departure: saturated nucleate boiling of FC-72, in: Proceedings of the 5th ASME/JSME Joint Thermal Engineering Conference, 1999 San Diego, California.
[15] 3M Corporation, 1995, 3M Fluorinert Liquids Product and Contact Guide.
[16] S.W. Churchill, H.H.S. Chu, Correlating equations for laminar and turbulent free convection from a vertical plate, Int. J. Heat Mass Transfer 18 (1975) 1323.
[17] S.J. Kline, F.A. McClintock, Describing uncertainties in single sample experiments, Mech. Eng. 75 (1953) 3–8.